DOI: 10.61782/fa.2025.0281

FORUM ACUSTICUM EURONOISE 2025

DESIGNING ACOUSTIC HOLOGRAMS WITHOUT IONISING RADIATION FOR WEARABLE TRANSCRANIAL ULTRASOUND THERAPY DEVICES

Alba Eroles-Simó[1*] **Víctor Vegas-Luque**[1] **Alicia Carrión**[1]
José A. Pineda-Pardo[2] **Juan J. Rodríguez-García**[1] **José L. Alonso-Ramos**[1]
Francisco Camarena[1] **Noé Jiménez**[1]

[1] Instituto de Instrumentación para Imagen Molecular (i3M), Universitat Politècnica de València (UPV) – Consejo Superior de Investigaciones Científicas (CSIC), Camino de Vera S/N, 46022 València, Spain

[2] HM CINAC (Centro Integral de Neurociencias Abarca Campal), Hospital Universitario HM Puerta del Sur, HM Hospitales, Madrid, 28938, Spain

ABSTRACT

Acoustic holograms are used in transcranial ultrasound to tailor the acoustic wavefront generated by a single-element transducer compensating skull aberrations and focusing the beam over brain structures. However, current hologram design relies on full-wave simulations where acoustic properties are known by computed tomography (CT). Since exposing patients to ionizing radiation is undesirable, we propose the use of zero echo time (ZTE) magnetic resonance images (MRI) to construct the patient-specific lens. This MRI sequence enables the visualization of tissues with short T2 values, such as bone. By establishing a linear correlation between CT Hounsfield Units (HU) and ZTE intensity values, pseudo-CT images are generated. Furthermore, transducer positioning has been optimised. Temporal bone window is established as a suitable surface for propagating acoustic waves, due to its reduced thickness and flat morphology. Results show that peak pressure at the focus is reduced by 5.38% when using pseudo-CT holograms respect to CT-holograms. The obtained treated volumes considering acoustic properties of the pseudo-CT and those of the CT show a difference of 0.18%. This approach can be applied in holographic wearable devices for transcranial ultrasound therapies such as blood-brain barrier opening or neuromodulation to avoid the use of ionising radiation during the therapeutic treatment.

Keywords: *therapeutic ultrasound, magnetic resonance imaging, neuromodulation, acoustic holograms, transtemporal window.*

1. INTRODUCTION

Therapeutic ultrasound is an emerging modality to treat diseases affecting the central nervous system. It represents a minimally invasive technique with high spatial resolution, which allows targeting even the innermost structures of the brain [1-3]. In those therapies, precise targeting accuracy is required to focus ultrasound energy on the desired structures inside the brain. However, the skull bones present high acoustic impedance, absorption, heterogeneity, and irregular thickness. These produce aberrations and defocusing of the acoustic beam due to strong scattering, reflection, refraction and attenuation effects [2,3]. To

[*] ***Corresponding author***: *aerosim@i3m.upv.es.*

mitigate these effects, acoustic holograms were proposed [4-6]. Acoustic holograms are passive lenses, commonly 3D printed, placed over a single-element transducer surface. They locally modulate the phase of the ultrasound beam, correcting skull aberrations and enabling the focalization over the desired structures inside the brain.

To design a lens for transcranial applications, full-wave acoustic simulations are performed, modelling wave propagation through the different media constituting the human head. These simulations require the acoustic properties of both soft tissues and cranial bones, which are commonly obtained from computed tomography (CT) images [7]. However, exposing patients to ionizing radiation is undesirable.

In this study, we propose the use of zero echo time (ZTE) magnetic resonance images (MRI) to avoid the use of X-ray CT images for hologram design. This imaging protocol enables the visualization of tissues with short T2 values, such as bone. Previous studies have obtained different linear correlations that enable ZTE intensity values conversion into Hounsfield Units (HU) measured on CT images. As a result, pseudo-CT images are obtained [8-11]. In addition, these pseudo-CT are used to optimize transducer location over the temporal bone window. With this approach, its flat morphology and reduced thickness are exploited, enabling higher pressure values at the focus, while reducing the remaining pressure over the skull [12,13]. This contributes to the optimal sonication of the desired structures inside the brain, allowing the generalisation and reproducibility of patient-specific positioning. It can be implemented in holographic wearable devices used in transcranial ultrasound therapies, eliminating the need for ionizing radiation.

2. METHODS

2.1 CT and ZTE Images

CT and ZTE images used in this work were obtained and provided by the Centro Integral de Neurociencias A.C. (HM CINAC) in Hospital Universitario HM Puerta del Sur and all patients provided written consent for data collection. The co-registration of both images is performed using 3DSlicer software. Density and sound velocity of hard and soft tissues are obtained from CT image values and the linear relationship between X-ray attenuation values.

2.1.1 Pseudo-CT Generation

To generate the pseudo-CT images, we have followed the steps presented by Miscouridou *et al.* [11]. ZTE images undergo a bias-field correction filter. Analysing the histogram of the resulting intensity values, two peaks can be identified. The first one, placed at lower intensity values, corresponds to the backward noise of the image. The second one, at higher intensity values, belongs to head soft tissues. Regarding this last peak, all voxel intensities are normalized to the soft tissue peak value. Intensity values between these two peaks are considered skull. By applying a threshold to the normalised ZTE image, a binary mask identifying the skull is generated. Morphological operations are used to fill the generated binary mask. Finally, the linear model defined in Eq. (1) is used in the voxels defined as skull, converting ZTE intensities values into HU [11].

$$CT = -2085\, ZTE + 2329. \qquad (1)$$

Fig. 1 shows the original HU values from the CT image and the HU values obtained from the transformation of the ZTE image into pseudo-CT for the same patient.

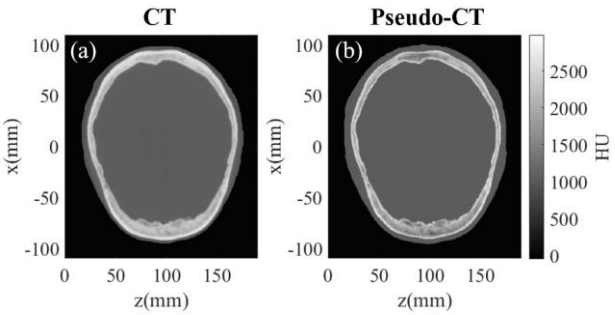

Figure 1. Representation of the HU values defined in (a) CT image, and the equivalent values obtained in (b) pseudo-CT.

2.2 Temporal Bone Window Positioning

An optimization algorithm has been developed to automate the positioning of the ultrasound transducer over the area of minimum thickness in the temporal window using the pseudo-CT [12,13]. In the sagittal view analysis of the generated skull mask, a local maximum in thickness can be identified in the temporomandibular joint (TMJ). Using the TMJ as a reference point, the algorithm automatically positions the transducer over the area of minimum thickness. To achieve normal orientation of the transducer with respect to the skin surface, it is necessary to ensure that there is no overlap with the ear structure [13].

2.3 Acoustic simulations

A flat transducer, with a diameter of 65 mm, excited at a central frequency of 650 kHz, is used. Skull, soft tissues and the transducer are considered to be immersed in water at a temperature of 37º C. Different acoustic simulations are performed in the time domain using MATLAB k-wave toolbox. It implements a pseudo-spectral method in k-space that allows the propagation of ultrasound in heterogeneous media to be modelled, considering the attenuation of the biological tissues considered. The defined workspace corresponds to a homogeneous medium, water, characterized as a cubic grid with a resolution of λ/6, where λ = 2.3 mm is the wavelength in water at the central frequency.

The holographic lens is designed performing a time-reversal simulation, known as *backward* simulation. A virtual source is placed at the centre of the therapeutic structure targeted for neuromodulation, the ventralis intermedius nucleus (Vim) of the thalamus. The segmented structure is corregistered for each analyzed patient. The virtual source emits a train of 100-cycle sinusoidal pulses at the central frequency. As the wavefront propagates through the skull, it is distorted due to differences in sound speed, density and attenuation, relative to those of soft tissues. The resulting wavefront is recorded over the holographic plane to design the geometry of the acoustic lens. Two different backward simulations are performed. The first one uses acoustic properties obtained from the CT image, while in the second one, the acoustic properties are extracted from the pseudo-CT image. As a result, two sets of holographic acoustic lenses are designed for each patient. An example of the recorded phase distribution over the holographic plane used to construct them is shown in Fig. 2.

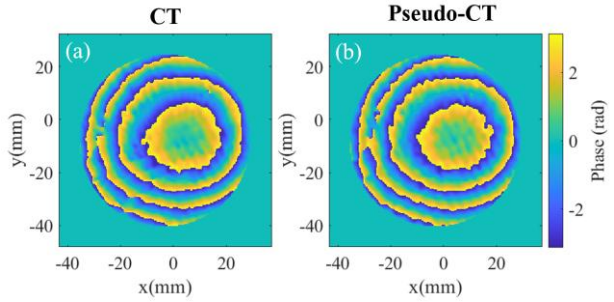

Figure 2. Phase distribution of the wavefront recorded in the holographic plane coming from the virtual source, taking into account the acoustic properties of (a) the CT image and (b) the pseudo-CT image.

In the numerical model, the material used for constructing the lens is a photoreactive resin Clear (Formlabs, USA) with the following acoustic properties: c_L = 2599.31 m/s, ρ_L = 1185.78 kg/m^3. The absorption value was set at α_L = 3.13 dB/(cm·MHz^y) at 650kHz, where y = 1.3, in agreement with values reported for photopolymers with similar properties [4].

A second acoustic simulation is then conducted, known as *forward* simulation. The same acoustic pulse is now emitted from the previously defined transducer. The wave passes through the holographic lens, which modulates it in phase, then through the skull, enabling the focalization over the desired structure. The maximum pressure acoustic field in the volume of interest is recorded for analysis. Three different situations are considered. First, the holographic lens designed using CT-derived acoustic properties is evaluated under matching conditions (CT-CT). Second, pseudo-CT based lens is measured under consistent acoustic conditions (pCT-pCT). Third, the pseudo-CT based lens performance is evaluated under CT acoustic properties in an effort to approximate the most realistic clinical scenario (pCT-CT).

3. RESULTS

The acoustic fields simulated under the specified conditions are evaluated in 5 anonymised patients. The differences between the resulting acoustic fields are quantified in terms of variations in focal position, volume of the sonicated therapeutic target, and peak pressures. In Fig. 3, the resulting acoustic fields obtained in the different considered situations are analysed, being (a) and (b) XZ and YZ planes for CT-CT, respectively, (c) and (d) for pCT-pCT, (e) and (f) for pCT-CT.

Fig. 4. (a) illustrates the deviation along the axial axis with respect to the coordinates of the virtual source defined for the holographic lens design, establishing that there is no significant difference between simulation conditions. A deviation of (-0.31 ± 1.80) mm along the beam propagation axis is observed between the pCT-CT and pCT-pCT simulations, while the deviation respect to CT-CT simulations is (1.02 ± 1.97) mm. Along the lateral axes, the deviation is not significantly distinguishable.

With respect to the sonicated target volume, the mean volume of the therapeutic target is (371.46 ± 5.20) mm^3. The results of the simulated fields show a reduction of 0.17% in the sonicated target volume when comparing the

pCT-CT to the pCT-pCT field. When comparing the treated volume between pCT-CT and CT-CT, the reduction is 0.18%.

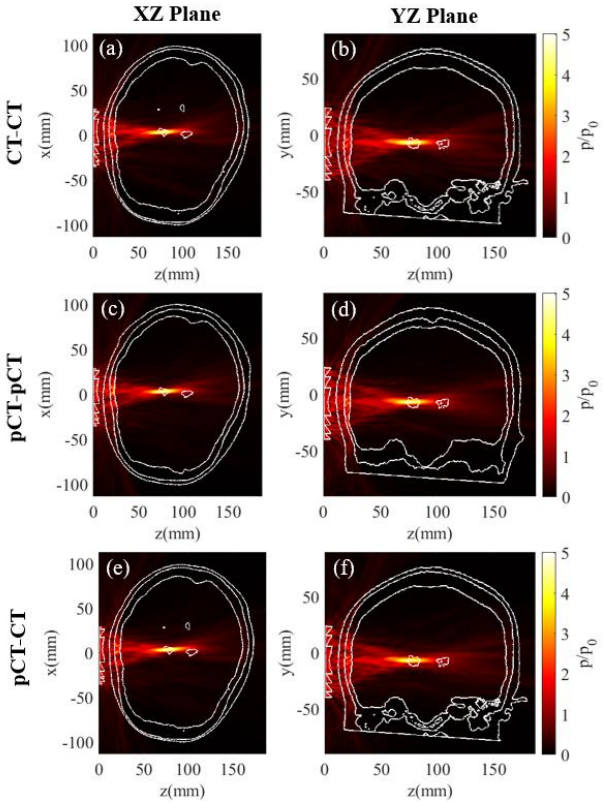

Figure 3. XY and YZ planes amplitude distribution of the acoustic field. (a) and (b) for the CT-CT simulation conditions, (c) and (d) for pCT-pCT conditions and (e) and (f) for the pCT-CT simulation conditions.

Regarding pressure values, a decrease of 3.74% in the maximum focal pressure is observed in pCT-CT field compared to the pCT-pCT field. When this same parameter is compared to the CT-CT field, the reduction reaches 5.38%. Fig. 4. (b) presents the mean maximum pressure measured at the focus for the 5 analysed patients under each simulation condition. Furthermore, the mean pressure over the analysed target volume is also evaluated. In the pCT-CT field, a decrease of 5.47% is measured relative to the pCT-pCT field, while a 5.57% reduction is observed when compared to CT-CT field. When optimizing transducer positioning, the remaining pressure over the skull is minimized. It can be seen that the maximum pressure on the skull in the pCT-CT field is reduced by 0.31%, yielding equivalent values to those obtained in the CT-CT field.

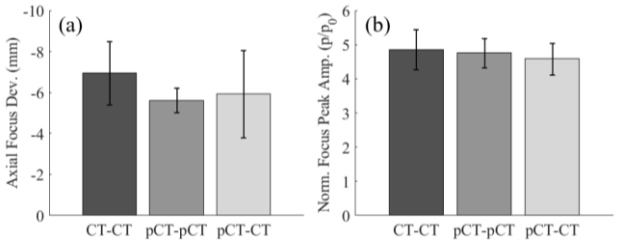

Figure 4. (a) Mean focus deviation in the beam propagation axis. (b) Mean normalized peak pressure measured at the beam focus. Kolmogorov-Smirnov test ($p>0.05$), establishes that there is no significant difference between pCT-pCT and pCT-CT, neither between CT-CT and pCT-CT.

4. CONCLUSION

By employing ZTE images, we generate pseudo-CT images that enable accurate estimation of skull acoustic properties. This study demonstrates that such images can be used as a suitable substitute for CT images in the design and fabrication of holographic lenses. They also allow the precise positioning over the temporal bone window.

Comparative analyses between the generated acoustic fields obtained using CT-based and pseudo-CT-based holographic lenses revealed that the treated volume remains constant. However, although not significant, differences in focal positioning and a reduction in the maximum pressure are observed. Future research will focus on correcting these variations by analyzing the potential underestimation of the skull HU values in pseudo-CT images.

These findings support the use of ZTE images as a non-ionizing alternative for the development of patient-specific acoustic holograms. Their integration into wearable transcranial ultrasound therapy devices opens a new path for non-invasive clinical applications, including neuromodulation and blood-brain barrier opening, while ensuring patient safety and the precision of the treatment.

5. ACKNOWLEDGMENTS

This research has been funded by Generalitat Valencia through grants INVEST/2023/553, EDGJID/2021/189, INNEST/2022/345 and CIAICO/2023/052. This research has been funded by the Minsterio Español de Ciencia e Innovación y el Ministerio de Universidades with grants PREP2022-000156 by the Agencia Estatal de Investigación,

PID2022-142719OB-C21 and CNS2023-145707 funded by MCIN/AEI/10.13039/501100011033 and by the FSE+.

6. REFERENCES

[1] J. Kubanek: "Neuromodulation with transcranial focused ultrasound," *Neurosurgical Focus*, vol. 44, no. 2, 2018.

[2] A. Fomenko and A.M. Lozano: "Neuromodulation and ablation with focused ultrasound – toward the future of noninvasive brain therapy," *Neural Regeneration Research*, vol. 14, no. 9, pp. 1509–1510, 2019.

[3] K. Lee, T.Y. Park, W. Lee and H. Kim: "A review of functional neuromodulation in humans using low intensity transcranial focused ultrasound," *Biomedical Engineering Letters*, vol. 14, pp. 407-438, 2024.

[4] K. Melde, A.G., Mark, T. Qiu and P. Fischer: "Holograms for acoustics," *Nature*, vol. 537, pp. 518-522, 2016.

[5] S. Jiménez-Gambín, N. Jiménez, J.M. Benlloch and F. Camarena: "Holograms to Focus Arbitrary Ultrasonic Fields through the Skull," *Physical Review Applied*, vol. 12, no. 1, 2019.

[6] D. Andrés, A. Carrión, F. Camarena and N. Jiménez: "Methods to design and evaluate transcranial ultrasonic lens using acoustic holography," *Physical Review Applied*, vol. 20, no. 4, 2023.

[7] J.F. Aubry, M. Tanter, M. Pernot, JL. Thomas and M. Fink: "Experimental demonstration of noninvasive transskull adaptive focusing based on prior computed tomography scans," *The Journal of the Acoustical Society of America*., vol. 113, no. 1, pp. 84-93, 2003.

[8] F. Wiesinger, L.I. Sacolick, A. Menini, S.S. Kaushik, S. Ahn, P. Veit-Haibach, G. Delso, D.D. Shanbhag: "Zero TE MR Bone Imaging in the Head," *Magnetic Resonance in Medicine*, vol. 75, pp. 107-114, 2016.

[9] F. Wiesinger, M. Bylund, J. Yang, S.S. Kaushik, D.D. Shanbhag, S. Ahn, J.H. Jonsson, J.A. Lundman, T. Hope, T. Nyholm, P. Larson, C. Cozzini: "Zero TE-based pseudo-CT image conversion in the head and its application in PET/MR attenuation correction and MR-guided radiation therapy planning," Magnetic Resonance in Medicine, vol. 80, pp. 1440-1451, 2018.

[10] J. Caballero-Insaurriaga, R. Rodríguez-Rojas, R. Martínez-Fernández, M. Del-Alamo, L. Díaz-Jiménez, M. Ávila, M. Martínez-Rodrígo, P. García-Polo and J.A. Pineda-Pardo: "Zero TE MRI Applications to Transcranial MR-Guided Focused Ultrasound: Patient Screening and Treatment Efficiency Estimation," *Journal of Magnetic Resonance Imaging*, vol. 50, no. 5, pp. 1583-1592, 2019.

[11] M. Miscouridou, J.A. Pineda-Pardo, C.J. Stagg, B.E. Treeby and A. Stanziola: "Classical and Learned MR to Pseudo-CT Mappings for Accurate Transcranial Ultasound Simulation," *IEEE Transactions on Ultrasonics, Ferroelectrics, and Frequency Control*, vol. 69, no. 10, pp.2896-2905, 2022.

[12] D. Andrés, N. Jiménez, J.M. Benlloch and F. Camarena: "Numerical Study of Acoustic Holograms for Deep-Brain Targeting through the Temporal Bone Window," *Ultrasound in Medicine & Biology*, vol. 48, no. 5, pp. 872-886, 2022.

[13] A. Eroles-Simó, D. Andrés, A. Carrión, J.J. Rodríguez-García, J.L. Alonso-Ramos, J.A. Pineda-Pardo, N. Jiménez and F. Camarena, "Optimización del posicionamiento de transductores de ultrasonidos sobre la ventana del hueso temporal," in *Conf. Proc. of Tecniacústica 2024-55º Congreso Español de Acústica y XIII Congreso Ibérico de Acústica*, (Faro, Portugal), pp. 637-645, 2024.